

Article

Neptunium Reactivity During Co-Precipitation and Oxidation of Fe(II)/Fe(III) (Oxyhydr)oxides

Hannah E. Roberts ¹, Katherine Morris ¹, J. Frederick W. Mosselmans ² , Gareth T. W. Law ³ and Samuel Shaw ^{1,*}

¹ Research Centre for Radwaste Disposal and Williamson Research Centre for Molecular Environmental Science, School of Earth, and Environmental Sciences, The University of Manchester, Manchester M13 9PL, UK; Hannah.Roberts@wsp.com (H.E.R.); katherine.morris@manchester.ac.uk (K.M.)

² Diamond Light Source Ltd., Diamond House, Harwell Science and Innovation Campus, Didcot, Oxfordshire OX11 0DE, UK; fred.mosselmans@diamond.ac.uk

³ Radiochemistry Unit, Department of Chemistry, The University of Helsinki, A.I. Virtasen Aukio 1 (PL 55), 00014 Helsinki, Finland; gareth.law@helsinki.fi

* Correspondence: sam.shaw@manchester.ac.uk; Tel.: +44-0161-275-3826

Received: 23 November 2018; Accepted: 14 December 2018; Published: 8 January 2019



Abstract: Fe(II) bearing iron (oxyhydr)oxides were directly co-precipitated with Np(V)O₂⁺ under anaerobic conditions to form Np doped magnetite and green rust. These environmentally relevant mineral phases were then characterised using geochemical and spectroscopic analyses. The Np doped mineral phases were then oxidised in air over 224 days with solution chemistry and end-point oxidation solid samples collected for further characterisation. Analysis using chemical extractions and X-ray absorption spectroscopy (XAS) techniques confirmed that Np(V) was initially reduced to Np(IV) during co-precipitation of both magnetite and green rust. Extended X-Ray Absorption Fine Structure (EXAFS) modelling suggested the Np(IV) formed a bidentate binuclear sorption complex to both minerals. Furthermore, following oxidation in air over several months, the sorbed Np(IV) was partially oxidised to Np(V), but very little remobilisation to solution occurred during oxidation. Here, linear combination fitting of the X-Ray Absorption Near Edge Structure (XANES) for the end-point oxidation samples for both mineral phases suggested approximately 50% oxidation to Np(V) had occurred over 7 months of oxidation in air. Both the reduction of Np(V) to Np(IV) and inner sphere sorption in association with iron (oxyhydr)oxides, and the strong retention of Np(IV) and Np(V) species with these phases under robust oxidation conditions, have important implications in understanding the mobility of neptunium in a range of engineered and natural environments.

Keywords: neptunium; magnetite; green rust; oxidation; XAS; XANES; EXAFS

1. Introduction

Neptunium (²³⁷Np) is an important transuranic radionuclide in higher activity radioactive wastes due to its long half-life (2.13×10^6 years), potentially high environmental mobility as Np(V), and significant radiotoxicity [1–4]. Its oxidation state is a key control on its environmental mobility [5]. Under oxidising conditions, the dioxygenyl neptunyl species (Np(V)O₂⁺) dominates with a high predicted mobility in the environment. In contrast, Np(IV) dominates under anaerobic conditions and is considered largely immobile due to the low solubility of hydrolysis products such as Np(IV)O₂ [6–8]. At alkaline pH, the solubility of metal ions including Np(V) and Np(IV) is expected to be low. As a result, many disposal concepts for intermediate level radioactive wastes use grouting with cement, which develops alkaline conditions intended to reduce the mobility and solubility of radionuclides in waste [9]. Additionally, intermediate level wastes are typically expected to be grouted in steel

canisters during storage and ultimately disposed within deep geological disposal facilities [10]. Here, corrosion of steel over extended time periods leads to formation of Fe(II) bearing (oxyhydr)oxides phases such as magnetite and green rust [11]. These phases have been shown to have extensive interactions with actinides [11–17]. In this context, understanding the behaviour of neptunium in the presence of Fe oxyhydroxides, including magnetite and green rust, informs prediction of the long-term behaviour of risk driving radionuclides in engineered and natural environments, including in radioactive waste disposal.

Previous studies demonstrate that Np(V) can interact with phases such as ferrihydrite [18–20], lepidocrocite [21], goethite [19,20,22], hematite [19,20,23] and magnetite [12,16,20,24]. Here, for Fe(III) containing minerals, Np(V) typically forms inner sphere Np(V) complexes or, in the presence of carbonate, Np(V)-carbonate surface complexes [19,23,25]. Additionally, recent work highlights that during transformation of ferrihydrite to hematite, Np(V) may be incorporated into hematite [19].

By contrast, in the presence of Fe(II) bearing mineral phases, past studies have reported that Np(V) is reduced to Np(IV) [12,13,16,24,26]. Initial work suggested enhanced removal of Np(V) to magnetite surfaces under anaerobic conditions, and chemical extractions suggested Np(IV) dominated [12,24]. Latterly, the reaction of Np(V) with pre-formed green rust sulphate was examined. This showed Np(V) was rapidly sorbed and reduced to Np(IV). The mechanism of reaction was postulated to be Np(V) sorption to the green rust surface and then reduction to discrete NpO₂ nanoparticles [13]. Upon oxidation of Fe(II) containing iron (oxyhydr)oxides, Np typically remains largely associated with the mineral phase, with the reduced Np(IV) withstanding the oxidation process for several weeks [13].

In contrast to Np(V), uranium as U(VI) reacts with Fe(II)-bearing (oxyhydr)oxides forming U(IV) surface complexes and/or precipitates [15,27]. In the interaction between U(VI) and magnetite at high concentrations, reduction to U(IV) is seen via two single electron transfer steps: UO₂²⁺ to UO₂⁺ and UO₂⁺ to U(IV)O₂ [15,28]. Indeed, the disproportionation of UO₂⁺ in solution under ambient conditions results in the formation of UO₂²⁺ and U(IV)O₂ [29]. More recently, UO₂²⁺ reduction in the presence of Fe(II) bearing (oxyhydr)oxides has been shown to stabilise U(V) through sorption or incorporation mechanisms [17,30–32].

Overall, there is a paucity of information concerning the reactivity of Np(V) with Fe(II) bearing (oxyhydr)oxide phases such as magnetite and green rust during their formation. Furthermore, the impact of oxidation on neptunium mobility is poorly defined with some reports of oxidative remobilisation [13], but with few studies examining the speciation of Np after oxidation. The aims of the current work were to determine the products formed during the direct co-precipitation of magnetite and green rust with Np(V) under alkaline and anaerobic conditions of relevance to radioactive waste disposal using the experimental approach described in Roberts et al. (2017) [17]. Additionally, the speciation and reactivity of Np was explored during the oxidation of the synthesised products. Solid samples were analysed using X-ray Absorption Spectroscopy (XAS), with XAS analyses being extended to dilute concentrations (tens–hundreds of ppm) of neptunium where possible. Latterly, sub-aliquots of the reduced, Np labelled magnetite and green rust were oxidised in air over several months. Parallel inactive experiments were performed to track mineral alteration using X-ray diffraction (XRD). The combination of XAS for Np speciation analyses informed by XRD analysis on inactive samples allowed us to define neptunium reactivity in these complex systems. Overall, this provided new insights into Np(V) speciation and fate on reaction with the environmentally relevant iron (oxyhydr)oxide mineral phases magnetite and green rust during reduction and oxidation.

2. Materials and Methods

A direct co-precipitation experiment was performed to synthesise magnetite and green rust at room temperature under anaerobic (Coy Cabinet, ~3% H₂: 97% N₂) conditions and in the presence of Np(V)O₂⁺ [17,33]. In brief, solutions of FeCl₂, FeCl₃, 0.3 M HCl, and Np(V) to yield a final concentration of Np on solids of approximately 30 or 300 ppm (approximately 400 Bq or 4000 Bq per experiment), were reacted under either magnetite (Fe(II)/Fe(III) = 0.6) or green rust (Fe(II)/Fe(III) = 2.0) formation

conditions [17]. The aqueous, acidified solutions were equilibrated under anaerobic conditions for 24 h before being introduced to a rapidly stirring, N₂ sparged 28–30% *w/v* NH₄OH solution (pH 11) to induce alkaline precipitation of magnetite or green rust [17]. The reaction products were then left to stir for several hours at pH 9 under anoxic conditions prior to solid samples being harvested for XAS analysis. At this stage, approximately 50% of the solution sample with magnetite or green rust present was centrifuged (4000 rpm, 5 min) and retained for analysis. The remaining 50% was used in oxidation experiments. Additionally, parallel non-active samples were synthesised and reacted under identical conditions (without neptunium) to allow mineralogical characterisation of the green rust and magnetite phases during co-precipitation of the fresh mineral phases and during oxidation. Oxidation of the samples was performed by removing the lid from the sample bottle in air and gently aerating the sample headspace by swirling for 1 min (approximately 1:5 solution to headspace ratio). The lid was then placed back on the bottle and the sample swirled for a further minute. Headspace aeration was repeated hourly during working hours during the first 2 days, followed by daily aeration for the following month and then approximately weekly aeration. Samples were taken during oxidation at day 0, 1, 8, 21 and 224, separated using centrifugation (14,000 × *g* 10 mins) and the solution phase acidified, diluted in 2% HNO₃, and analysed using ICP-MS to monitor the total neptunium concentration in solution. XRD samples and pH readings were also taken from the parallel, non-active samples during this time to document mineralogical and geochemical changes. XRD analysis was performed on a Bruker D8 ($\lambda = \text{Cu K-}\alpha 1$) diffractometer. Neptunium L₃-edge spectroscopy data were collected on mineral pastes at beamline I20 at Diamond Light Source under fluorescent mode using either a 36 or 64 Ge element detector and at room temperature [34]. During data acquisition we assessed the potential for beam induced oxidation state changes and did not observe any evidence of beam induced effects. The scanning branch of the I20 beamline offers key capability to enable the collection of high quality EXAFS data from low concentration samples ([35]). The wiggler source provides high levels of flux ($>10^{12}$ photons per second). The combination of flux and detector configuration allows the collection of high-quality EXAFS from low concentration samples. Data analyses were performed using Athena and Artemis using Feff8 [36]. The statistical validity of the addition of all scattering paths was evaluated using the F-test for EXAFS [37].

3. Results and Discussion

Analysis of XRD patterns for the parallel, non-active samples on mineral co-precipitation confirmed magnetite (Fe(II)/Fe(III) = 0.6) and green rust (Fe(II)/Fe(III) = 2.0) to be the dominant products formed during co-precipitation (Figure 1). Mineralogical changes were also tracked throughout the oxidation of the iron (oxyhydr)oxides in these samples (Figure 1). Here, on initial oxidation (day 1), magnetite was observed as the dominant mineral phase in Fe(II)/Fe(III) = 0.6 as well as minor contributions from oxidised Fe(II) mineral phases including maghemite, lepidocrocite and goethite. For Fe(II)/Fe(III) = 2.0, green rust had fully oxidised to magnetite by day 1. During the period of oxidation, from day 0 to day 8 the proportion of magnetite/maghemite, goethite and lepidocrocite increased with the oxidised minerals present over the 224 days of reoxidation. Similarly, the relatively slow oxidation of magnetite to Fe(III) (oxyhydr)oxides has also been seen in Tc-magnetite oxidation experiments [38].

During direct mineral co-precipitation, the aqueous phase concentration of Np was tracked after separation of the solid and solution phase with centrifugation (14,000 × *g*, 10 mins) and acidification into 2% HNO₃ using ICP-MS. Here, during both magnetite and green rust formation, Np(V) was essentially completely removed to solids under the pH 9, mildly alkaline end point (solution concentration <10 ppt Np). Additionally, during oxidation of both magnetite and green rust where the pH decreased slightly to pH 8, solution analyses showed Np had a very high continued affinity for the iron (oxyhydr)oxide mineral phases as they underwent oxidation over 224 days again with a solution concentration <10 ppt Np. This is consistent with the iron oxides having a high sorption capacity for neptunium under the experimental conditions [19,39].

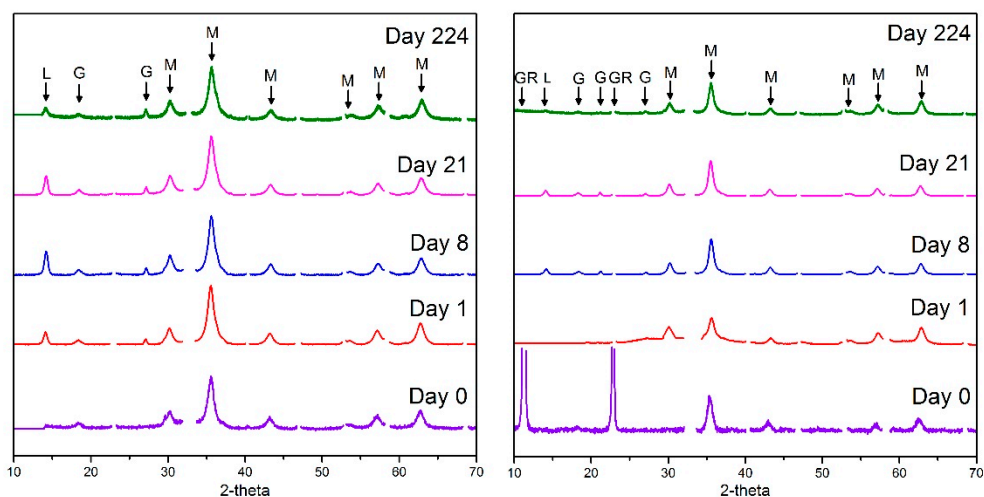


Figure 1. X-ray diffraction (XRD) pattern time series for Fe(II)/Fe(III) = 0.6 and Fe(II)/Fe(III) = 2.0 over a period of oxidation in air from time 0 (freshly co-precipitated) to 224 days. Observable peaks are indexed with GR, M, L or G indicating green rust, magnetite, lepidocrocite or goethite, respectively.

To further define the speciation of neptunium in the co-precipitated mineral phases upon their formation and subsequent oxidation, neptunium L₃ edge XANES and EXAFS spectra were collected on the solid phase samples at the reduction and oxidation endpoints. The Np concentration on the solids was between 30 and 300 ppm. In the magnetite system we worked with dilute (tens of ppm) concentrations of Np to start to explore the limits of XAS analyses, both to reach into more environmentally relevant concentrations and to reduce radiotoxicity in experiments. Samples analysed included co-precipitated magnetite (30 and 300 ppm), co-precipitated green rust (300 ppm), end-point oxidised magnetite (300 ppm, 224 days oxidation) and end-point oxidised green rust (300 ppm, 224 days oxidation).

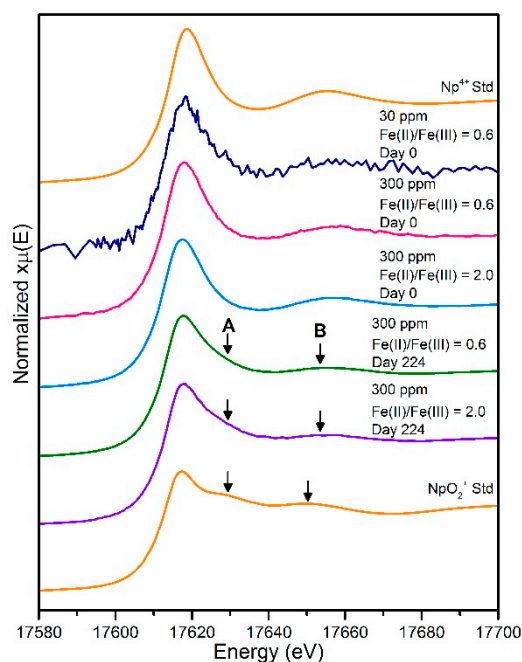


Figure 2. Neptunium L₃ edge XANES spectra collected from 30 ppm and 300 ppm reduced samples and for 300 ppm samples post oxidation (day 224). Reference spectra for aqueous Np⁴⁺ and aqueous neptunyl (NpO₂⁺) are shown for comparison [40]. Arrows indicate the positions of the resonance features of the XANES for A) axial Np-O and B) equatorial Np-O.

In the freshly co-precipitated magnetite and green rust samples, XANES spectra for the magnetite 30 and 300 ppm and green rust 300 ppm Np samples clearly resembled the Np(IV) standard and confirmed reduction to Np(IV) was occurring (Figure 2). We further note the 30 ppm Np XANES sample provided clear XANES information regarding reduction to Np(IV) at this very low element concentration. The data provide a link between elevated and more environmentally relevant concentrations and present a positive prospect for dilute transuranic analyses in this type of sample. The 224 day end-point samples from oxidation of both magnetite and green rust samples at 300 ppm show XANES which suggest partial oxidation from a Np(IV)-like spectrum to a more mixed Np(IV)/Np(V)-like spectrum (Figure 2). For example, in both the magnetite and green rust end-point oxidation Np XANES, there was a clear increase in the dioxygenyl axial resonance feature (A; Figure 2) in the spectra when compared to the freshly co-precipitated phases (Figure 2). In order to further quantify the extent of Np(IV) and Np(V) in the samples, linear combination fitting of the XANES between the reduced Np(IV) from the freshly co-precipitated magnetite sample and Np(V) sorbed to iron oxide [19] was performed. Here, the linear combination fits were consistent between the two samples and suggested that approximately 50–60% of the Np was oxidised to Np(V) in both the magnetite and green rust samples after 224 days (Table 1).

Table 1. Linear combination fitting results for XANES samples Fe(II)/Fe(III) = 0.6 and Fe(II)/Fe(III) = 2.0 at 300 ppm after oxidation. Fitting was performed using a Np(V) ferrihydrite standard [19] and the Fe(II)/Fe(III) = 0.6, 300 ppm sample before oxidation for Np(IV).

	Component 1: Np(V) (%)	Component 2: Np(IV) (%)
Fe(II)/Fe(III) = 0.6, magnetite: 300 ppm Day 224	53	47
Fe(II)/Fe(III) = 2.0, green rust: 300 ppm Day 224	60	40

Neptunium L₃- edge EXAFS data were also collected and analysed for the freshly co-precipitated magnetite and green rust solid samples for the 300 ppm experiments as well as the 224 day, 300 ppm oxidation solids from both mineral systems (Figure 3, Table 1). For the freshly co-precipitated samples, EXAFS fitting was informed by published models for Np(IV) reduction products [4,7,16,41]. Here, the EXAFS spectra for both of the co-precipitation products were, within data quality constraints, remarkably consistent and could both be fitted with a model of 7 oxygens at 2.31–2.38 Å, consistent with a Np(IV) like coordination environment [7,41]. Indeed, the Np–O path length for the freshly co-precipitated magnetite sample was consistent with that reported for Np(IV) sorption to titanomagnetite [16]. Modelling of additional features in the EXAFS was again informed by the relevant literature and we considered the potential for Fe to be contributing to an additional backscattering shell at approximately 3.4 Å [4,16,42]. Here, the best fit for both magnetite and green rust suggested that additional 2 Fe backscatterers between 3.41–3.49 Å were statistically valid for both of the samples. Again, this was consistent with Np–Fe bond distances reported for Fe (oxyhydr)oxide interactions, including with titanomagnetite [16], although in our sample, the number of backscattering Fe atoms in the fit was much lower than in the titanomagnetite work. This confirms adsorption of the Np(IV) via an inner sphere, bidentate binuclear complex to both the magnetite and green rust during direct co-precipitation. Indeed, this coordination is often seen in magnetite with different cations [43–45]. Similar Np adsorption mechanisms to mineral surfaces have also been seen in iron (oxyhydr)oxide phases, including observations of the bidentate, mononuclear complexation of Np(V) to hematite and ferrihydrite [19,25]. Interestingly, in the current study, there was no strong evidence for a significant Np–Np interaction in the EXAFS at approximately 3.8 Å (although it is possible this is a consequence of the limited data range). Its absence (within the data range constraints for these samples) suggests that nano-crystalline NpO₂ may not be a dominant reaction product in this system and in contrast to recent studies [7,46]. In U(VI)O₂²⁺ sorption experiments with magnetite, U(IV) monodentate surface complexes formed at low U concentrations, whilst at higher concentrations (approximately 20,000 ppm U), nanocrystalline uraninite (UO₂) was favoured [15]. In the current study, at low

(300 ppm) concentrations, Np(IV) speciation is dominated by a monodentate binuclear complex, and (within data quality constraints) there is little evidence for significant NpO_2 formation. This is consistent with the observations of Wylie et al. (2016) [16].

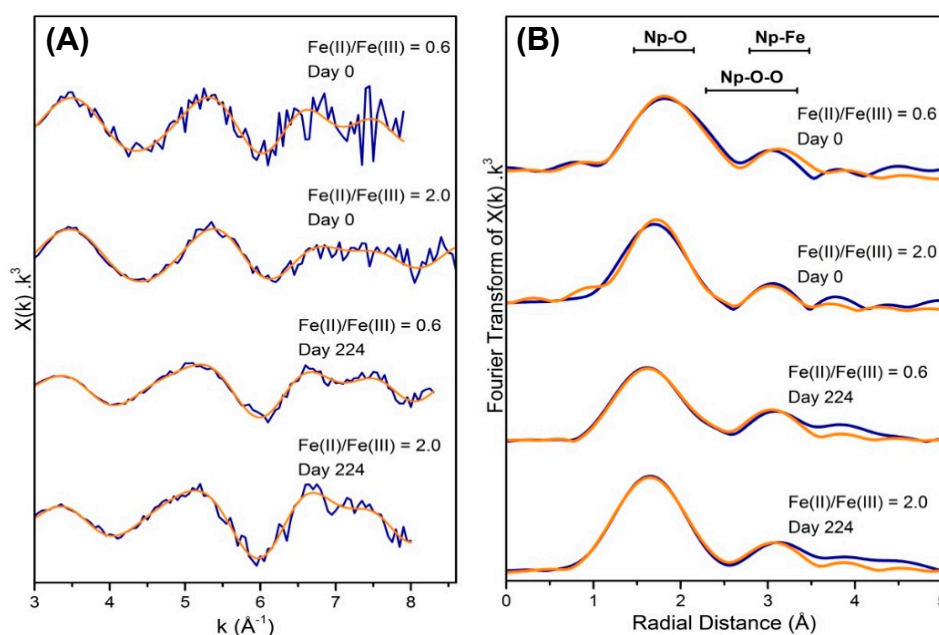


Figure 3. (A) Neptunium L_3 -edge EXAFS spectra and (B) corresponding Fourier transforms of the EXAFS data for both Fe(II)/Fe(III) = 0.6 (magnetite) and Fe(II)/Fe(III) = 2.0 (green rust) samples for freshly co-precipitated samples and for 224 day oxidised samples at approximately 300 ppm neptunium. Blue lines are k^3 -weighted data and orange lines are best fits to the data.

On oxidation there was evidence for partial oxidation of the Np(IV) to neptunyl Np(V) from the XANES spectra (Figure 2) with linear combination fitting indicating approximately 50–60% oxidation to Np(V) (Table 1). For the EXAFS, fitting was informed by both the XANES linear combination fits suggesting partial oxidation and by relevant literature for Np(V) neptunyl and Np(IV) O_2 coordination environments [7,19,46]. For the oxidised samples, a good fit was obtained assuming the ratio of Np(IV) to Np(V) suggested by the XANES linear combination fitting for each of the samples. There was not enough data to refine these occupancy numbers further, and hence, they were fixed at 1.06 and 1.2 for the short (axial, neptunyl) O path and 5.94 and 5.8 for the more distant O in the oxidised magnetite and green rust samples respectively. This resulted in Np–O interactions at 1.86 \AA and 2.36 \AA for the oxidised magnetite samples and 1.88 \AA and 2.39 \AA for the oxidised green rust samples (Table 2). These distances are consistent with axial Np–O distances in Np(V) and both equatorial Np(V) and Np–O distances in Np(IV) [4,7,16,19,23,25]. Multiple scattering paths were present in both oxidised samples, which arise as a result of scattering within the linear Np(V) dioxygenyl actinyl ions, again confirming the presence of Np(V) dioxygenyl in the samples [47–49]. Finally, the presence of 1.5–1.9 Fe-backscatterers at approximately 3.46 \AA was fitted for both oxidation samples with good confidence and consistent with inner sphere adsorption dominating for the Np species after extensive oxidation of these samples (Table 2).

Overall, the XANES suggests and the EXAFS are consistent with a mixture of adsorbed Np(IV) and Np(V) present on oxidation. Furthermore, within the constraints of the data set, there was no clear evidence for incorporation of Np(V) in either the freshly formed co-precipitates or the oxidation products. For the freshly formed co-precipitates, the absence of Np(V) incorporation into magnetite or green rust is in contrast to the recently observed reduction of U(VI) to U(V) and its subsequent incorporation and stabilisation in these phases in a U(V), uranate-like coordination environment [17,30]. For the oxidation products, the lack of clear evidence for Np(V) incorporation into the oxidised Fe(III)

bearing (oxyhydr)oxide phases is in contrast to recent work where Np(V) incorporation into hematite has been observed [19]. In fact, the fitting for the oxidation samples indicates that the dioxygenyl axial oxygen bond lengths were largely retained in this system. Furthermore, there was no evidence for the extensive Fe backscatterers seen from 2.88–3.57 Å, observed during Np(V) incorporation to Fe-oxides where neptunate-like speciation facilitates incorporation into the crystal lattice [19].

Table 2. Details of EXAFS best fit parameters for Fe(II)/Fe(III) = 0.6 (magnetite) and Fe(II)/Fe(III) = 2.0 (green rust) samples at 300 ppm neptunium before and after oxidation.

Sample	Path	CN	R (Å)	$\sigma^2(\text{Å}^2)$	Confidence (%)	ΔE_0 (eV)	S_0^2	R	$\frac{\text{Variables}}{\text{NDP}}$
0.6, Day 0	Np-O	7	2.38(1)	0.016(1)	99	9.0	1 **	0.006	$\frac{7}{7.67}$
	Np-Fe	2	3.49(2)	0.005(2)					
2.0, Day 0	Np-O	7	2.31(2)	0.016(1)	97	3.9	1 **	0.009	$\frac{7}{8.16}$
	Np-Fe	2	3.41(3)	0.012(4)					
0.6, Day 224	Np-O	1.06 *	1.86(1)	0.005(1)	94	9.5	1 **	0.012	$\frac{8}{8.77}$
	Np-O	5.94 *	2.36(1)	0.023(1)					
	Np-Fe	1.9(5)	3.47(3)	0.008(2)					
	Np-O-O	1.06 *	3.72(2)	0.009(2)					
2.0, Day 224	Np-O	1.2 *	1.88(1)	0.001(1)	88	9.4	1 **	0.004	$\frac{8}{8.31}$
	Np-O	5.8 *	2.39(4)	0.017(2)					
	Np-Fe	1.5(5)	3.45(2)	0.002(2)					
	Np-O-O	1.2 *	3.76(2)	0.002(2)					

* Number of oxygen paths fixed according to XANES LCF results as data range was too short to vary these. ** S_0^2 was fixed at 1 during refinement.

4. Environmental Significance

In this study, the fate of Np(V) at low concentrations (30–300 ppm) during interactions with Fe(II)/Fe(III)-bearing (oxyhydr)oxides has been defined during the co-precipitation of magnetite and green rust and during the oxidation of these reduced mineral phases. Specifically we demonstrated the ability of Fe(II) containing mineral phases to reduce Np(V) in mildly alkaline conditions and form a bidentate binuclear Np(IV) sorption complex in both mineral systems. On oxidation of the minerals, there was significant but not complete oxidation of the reduced mineral phases. Interestingly, both Np(IV) and Np(V) were strongly retained on the oxidation products as inner sphere sorption complexes. Overall, this study provides new information on the interactions of Np(V) during its co-precipitation with magnetite and green rust and presents a positive prospect for low neptunium mobility in engineered and natural environments where Fe(II)-bearing Fe (oxyhydr)oxides exist.

Author Contributions: H.E.R.—principal author, mineral synthesis, radiochemistry and associated geochemical (ICP) and mineralogical (XRD, XAS) analysis; S.S.—conceptual guidance, XAS data modelling and extensive manuscript review; K.M.—conceptual guidance, XAS data modelling and extensive manuscript review; G.T.W.L.—conceptual guidance; J.F.W.M.—XAS data modelling.

Funding: This work was supported by the STFC (ST/L502534/1), ENV-RAD-NET (ST/K001787/1 and ST/N002474/1) and BIGRAD (NE/H007768/1).

Acknowledgments: We thank Diamond Light Source (SP13559) for beamtime. We thank Sofia Diaz-Moreno and Shu Hayama for support on I20 and Richard Doull for assistance with radiological samples at Diamond Light Source, John Waters for help with XRD, Carolyn Pearce for help with the mineral synthesis method, and Kathleen Law for assistance with Np(V) stock preparation.

Conflicts of Interest: the authors declare no conflicts of interest.

References

1. Thompson, R.C. Neptunium: The Neglected Actinide: A Review of the Biological and Environmental Literature. *Radiat. Res.* **1982**, *90*, 1–32. [CrossRef] [PubMed]
2. Nenot, J.C. Metabolism and Toxicity of Neptunium. Available online: https://inis.iaea.org/search/search.aspx?orig_q=RN:15061349 (accessed on 23 November 2018).

3. Kaszuba, J.P.; Runde, W.H. The Aqueous Geochemistry of Neptunium: Dynamic Control of Soluble Concentrations with Applications to Nuclear Waste Disposal. *Environ. Sci. Technol.* **1999**, *33*, 4427–4433. [[CrossRef](#)]
4. Law, G.T.W.; Geissler, A.; Lloyd, J.R.; Livens, F.R.; Boothman, C.; Begg, J.D.C.; Denecke, M.A.; Rothe, J.; Dardenne, K.; Burke, I.T.; et al. Geomicrobiological redox cycling of the transuranic element neptunium. *Environ. Sci. Technol.* **2010**, *44*, 8924–8929. [[CrossRef](#)] [[PubMed](#)]
5. Silva, R.J.; Nitsche, H. Actinide environmental chemistry. *Radiochim. Acta* **1995**, *70–71*, 377–396. [[CrossRef](#)]
6. Newsome, L.; Morris, K.; Lloyd, J.R. The biogeochemistry and bioremediation of uranium and other priority radionuclides. *Chem. Geol.* **2014**, *363*, 164–184. [[CrossRef](#)]
7. Brookshaw, D.R.; Patrick, R.A.D.; Bots, P.; Law, G.T.W.; Lloyd, J.R.; Mosselmans, J.F.W.; Vaughan, D.J.; Dardenne, K.; Morris, K. Redox Interactions of Tc(VII), U(VI), and Np(V) with Microbially Reduced Biotite and Chlorite. *Environ. Sci. Technol.* **2015**, *49*, 13139–13148. [[CrossRef](#)] [[PubMed](#)]
8. Thorpe, C.L.; Morris, K.; Lloyd, J.R.; Denecke, M.A.; Law, K.A.; Dardenne, K.; Boothman, C.; Bots, P.; Law, G.T.W. Neptunium and manganese biocycling in nuclear legacy sediment systems. *Appl. Geochem.* **2015**, *63*, 303–309. [[CrossRef](#)]
9. Cantrell, K.J.; Um, W.; Williams, B.D.; Bowden, M.E.; Gartman, B.; Lukens, W.W.; Buck, E.C.; Mausolf, E.J. Chemical stabilization of Hanford tank residual waste. *J. Nucl. Mater.* **2014**, *446*, 246–256. [[CrossRef](#)]
10. Morris, K.; Law, G.T.W.; Bryan, N.D. Geodisposal of Higher Activity Wastes. In *Nuclear Power and the Environment*; Harrison, R.M., Hester, R.E., Eds.; Royal Society of Chemistry: Cambridge, UK, 2011; pp. 129–151.
11. Dodge, C.J.; Francis, A.J.; Gillow, J.B.; Halada, G.P.; Eng, C.; Clayton, C.R. Association of uranium with iron oxides typically formed on corroding steel surfaces. *Environ. Sci. Technol.* **2002**, *36*, 3504–3511. [[CrossRef](#)] [[PubMed](#)]
12. Nakata, K.; Nagasaki, S.; Tanaka, S.; Sakamoto, Y.; Tanaka, T.; Ogawa, H. Sorption and reduction of neptunium(V) on the surface of iron oxides. *Radiochim. Acta* **2002**, *90*, 665–669. [[CrossRef](#)]
13. Christiansen, B.C.; Geckeis, H.; Marquardt, C.M.; Bauer, A.; Römer, J.; Wiss, T.; Schild, D.; Stipp, S.L.S. Neptunyl (Np) interaction with green rust. *Geochim. Cosmochim. Acta* **2011**, *75*, 1216–1226. [[CrossRef](#)]
14. Kirsch, R.; Fellhauer, D.; Altmaier, M.; Neck, V.; Rossberg, A.; Fanghanel, T.; Charlet, L.; Scheinost, A.C. Oxidation state and local structure of plutonium reacted with magnetite, mackinawite, and chukanovite. *Environ. Sci. Technol.* **2011**, *45*, 7267–7274. [[CrossRef](#)]
15. Latta, D.E.; Mishra, B.; Cook, R.E.; Kemner, K.M.; Boyanov, M.I. Stable U(IV) complexes form at high-affinity mineral surface sites. *Environ. Sci. Technol.* **2014**, *48*, 1683–1691. [[CrossRef](#)] [[PubMed](#)]
16. Wylie, E.M.; Olive, D.T.; Powell, B.A. Effects of Titanium Doping in Titanomagnetite on Neptunium Sorption and Speciation. *Environ. Sci. Technol.* **2016**, *50*, 1853–1858. [[CrossRef](#)] [[PubMed](#)]
17. Roberts, H.E.; Morris, K.; Law, G.T.L.; Mosselmans, J.F.W.; Bots, P.; Kvashnina, K.O.; Shaw, S. Uranium(V) incorporation mechanisms and stability in Fe(II)/Fe(III) iron (oxyhydr)oxides. *Environ. Sci. Technol. Lett.* **2017**, *4*, 421–426. [[CrossRef](#)]
18. Girvin, D.C.; Ames, L.L.; Schwab, A.P.; McGarrah, J.E. Neptunium adsorption on synthetic amorphous iron oxyhydroxide. *J. Colloid Interface Sci.* **1991**, *141*, 67–78. [[CrossRef](#)]
19. Bots, P.; Shaw, S.; Law, G.T.W.; Marshall, T.A.; Mosselmans, J.F.W.; Morris, K. Controls on the Fate and Speciation of Np(V) during Iron (Oxyhydr)oxide Crystallization. *Environ. Sci. Technol.* **2016**, *50*, 3382–3390. [[CrossRef](#)]
20. Li, D.; Kaplan, D.I. Sorption coefficients and molecular mechanisms of Pu, U, Np, Am and Tc to Fe (hydr)oxides: A review. *J. Hazard. Mater.* **2012**, *243*, 1–18. [[CrossRef](#)] [[PubMed](#)]
21. Yang, C.; Powell, B.A.; Zhang, S.; Rao, L. Surface complexation modeling of neptunium(V) sorption to lepidocrocite (γ -FeOOH). *Radiochim. Acta* **2015**, *103*, 707–717. [[CrossRef](#)]
22. Combes, J.M.; Chisholm-Brause, C.J.; Brown, G.E.; Parks, G.A.; Conradson, S.D.; Eller, P.G.; Triay, I.R.; Hobart, D.E.; Meijer, A.; Chisholm-Brause, C.J.; et al. EXAFS Spectroscopic Study of Neptunium(V) Sorption at the alpha-FeOOH/Water Interface. *Environ. Sci. Technol.* **1992**, *26*, 376–382. [[CrossRef](#)]
23. Müller, K.; Gröschel, A.; Rossberg, A.; Bok, F.; Franzen, C.; Brendler, V.; Foerstendorf, H. In situ spectroscopic identification of neptunium(V) inner-sphere complexes on the hematite-water interface. *Environ. Sci. Technol.* **2015**, *49*, 2560–2567. [[CrossRef](#)] [[PubMed](#)]

24. Nakata, K.; Nagasaki, S.; Tanaka, S.; Sakamoto, Y.; Tanaka, T.; Ogawa, H. Reduction rate of neptunium(V) in heterogeneous solution with magnetite. *Radiochim. Acta* **2004**, *92*, 145–149. [[CrossRef](#)]
25. Arai, Y.; Moran, P.B.; Honeyman, B.D.; Davis, J.A. In situ spectroscopic evidence for neptunium(V)-carbonate inner-sphere and outer-sphere ternary surface complexes on hematite surfaces. *Environ. Sci. Technol.* **2007**, *41*, 3940–3944. [[CrossRef](#)] [[PubMed](#)]
26. Bach, D.; Christiansen, B.C.; Schild, D.; Geckeis, H. Tem study of green rust sodium sulphate ($\text{GR}_{\text{Na},\text{SO}_4}$) Interacted with Neptunyl Ions (NpO_2^+). *Radiochim. Acta* **2014**, *102*, 279–289. [[CrossRef](#)]
27. Latta, D.E.; Pearce, C.I.; Rosso, K.M.; Kemner, K.M.; Boyanov, M.I. Reaction of UVI with Titanium-Substituted Magnetite: Influence of Ti on UIV Speciation. *Environ. Sci. Technol.* **2013**, *47*, 4121–4130. [[CrossRef](#)]
28. Harris, W.E.; Kolthoff, I.M. The Polarography of Uranium. III. Polarography in Very Weakly Acid, Neutral or Basic Solution. *J. Am. Chem. Soc.* **1946**, *62*, 446–451.
29. Ekstrom, A. Kinetics and mechanism of the Disproportionation of Uranium (V). *Inorg. Chem.* **1974**, *13*, 2237–2241. [[CrossRef](#)]
30. Pidchenko, I.; Kvashnina, K.O.; Yokosawa, T.; Finck, N.; Bahl, S.; Schild, D.; Polly, R.; Bohnert, E.; Rossberg, A.; Göttlicher, J.; et al. Uranium Redox Transformations after U(VI) Coprecipitation with Magnetite Nanoparticles. *Environ. Sci. Technol.* **2017**, *51*, 2217–2225. [[CrossRef](#)]
31. Skomurski, F.N.; Ilton, E.S.; Engelhard, M.H.; Arey, B.W.; Rosso, K.M. Heterogeneous reduction of U^{6+} by structural Fe^{2+} from theory and experiment. *Geochim. Cosmochim. Acta* **2011**, *75*, 7277–7290. [[CrossRef](#)]
32. Ilton, E.S.; Boily, J.F.; Buck, E.C.; Skomurski, F.N.; Rosso, K.M.; Cahill, C.L.; Bargar, J.R.; Felmy, A.R. Influence of Dynamical Conditions on the Reduction of UVI at the Magnetite-Solution Interface. *Environ. Sci. Technol.* **2010**, *44*, 170–176. [[CrossRef](#)]
33. Pearce, C.I.; Qafoku, O.; Liu, J.; Arenholz, E.; Heald, S.M.; Kukkadapu, R.K.; Gorski, C.A.; Henderson, C.M.B.; Rosso, K.M. Synthesis and properties of titanomagnetite ($\text{Fe}_{3-x}\text{Ti}_x\text{O}_4$) nanoparticles: A tunable solid-state Fe(II/III) redox system. *J. Colloid Interface Sci.* **2012**, *387*, 24–38. [[CrossRef](#)]
34. Diaz-Moreno, S.; Hayama, S.; Amboage, M.; Freeman, A.; Sutter, J.; Duller, G. I20; The Versatile X-ray Absorption spectroscopy beamline at Diamond Light Source. *J. Phys. Conf. Ser.* **2009**, *190*, 12038. [[CrossRef](#)]
35. Diaz-Moreno, S.; Amboage, M.; Basham, M.; Boada, R.; Bricknell, N.E.; Cibir, G.; Cobb, T.M.; Filik, J.; Freeman, A.; Geraki, K.; et al. The Spectroscopy Village at Diamond Light Source. *J. Synchrotron Radiat.* **2018**, *25*, 998–1009. [[CrossRef](#)]
36. Ravel, B.; Newville, M. ATHENA, ARTEMIS, HEPHAESTUS: Data analysis for X-ray absorption spectroscopy using IFEFFIT. *J. Synchrotron Radiat.* **2005**, *12*, 537–541. [[CrossRef](#)] [[PubMed](#)]
37. Downward, L.; Booth, C.H.; Lukens, W.W.; Bridges, F. A variation of the F-test for determining statistical relevance of particular parameters in EXAFS fits. *AIP Conf. Proc.* **2007**, *882*, 129–131. [[CrossRef](#)]
38. Marshall, T.A.; Morris, K.; Law, G.T.W.; Mosselmans, J.F.W.; Bots, P.; Parry, S.A.; Shaw, S. Incorporation and retention of 99-Tc(IV) in magnetite under high pH conditions. *Environ. Sci. Technol.* **2014**, *48*, 11853–11862. [[CrossRef](#)] [[PubMed](#)]
39. Romanchuk, A.Y.; Kalmykov, S.N. Actinides sorption onto hematite: Experimental data, surface complexation modeling and linear free energy relationship. *Radiochim. Acta* **2014**, *102*, 303–310. [[CrossRef](#)]
40. Hennig, C.; Ikeda-Ohno, A.; Tsushima, S.; Seheinost, A.C. The sulfate coordination of Np(IV), Np(V), and Np(VI) in aqueous solution. *Inorg. Chem.* **2009**, *48*, 5350–5360. [[CrossRef](#)]
41. Husar, R.; Weiss, S.; Hennig, C.; Hübner, R.; Ikeda-Ohno, A.; Zänker, H. Formation of neptunium(IV)-silica colloids at near-neutral and slightly alkaline pH. *Environ. Sci. Technol.* **2014**, *49*, 665–671. [[CrossRef](#)]
42. Williamson, A.J.; Morris, K.; Boothman, C.; Dardenne, K.; Law, G.T.W.; Lloyd, J.R. Microbially mediated reduction of Np(V) by a consortium of alkaline tolerant Fe(III)-reducing bacteria. *Mineral. Mag.* **2015**, *79*, 1287–1295. [[CrossRef](#)]
43. Missana, T.; García-Gutiérrez, M.; Fernández, V. Uranium (VI) sorption on colloidal magnetite under anoxic environment: Experimental study and surface complexation modelling. *Geochim. Cosmochim. Acta* **2003**, *67*, 2543–2550. [[CrossRef](#)]
44. Zhang, M.; Pan, G.; Zhao, D.; He, G. XAFS study of starch-stabilized magnetite nanoparticles and surface speciation of arsenate. *Environ. Pollut.* **2011**, *159*, 3509–3514. [[CrossRef](#)] [[PubMed](#)]
45. Pinakidou, F.; Katsikini, M.; Simeonidis, K.; Kaprara, E.; Paloura, E.C.; Mitrakas, M. On the passivation mechanism of Fe_3O_4 nanoparticles during Cr(VI) removal from water: A XAFS study. *Appl. Surf. Sci.* **2016**, *360*, 1080–1086. [[CrossRef](#)]

46. Husar, R.; Hübner, R.; Hennig, C.; Martin, P.M.; Chollet, M.; Weiss, S.; Stumpf, T.; Zänker, H.; Ikeda-Ohno, A. Intrinsic formation of nanocrystalline neptunium dioxide under neutral aqueous conditions relevant to deep geological repositories. *Chem. Commun.* **2015**, *51*, 1301–1304. [[CrossRef](#)] [[PubMed](#)]
47. Farges, F.; Ponader, C.W.; Calas, G.; Brown, G.E. Structural environments of incompatible elements in silicate glass/melt systems: II. UIV, UV, and UVI. *Geochim. Cosmochim. Acta* **1992**, *56*, 4205–4220. [[CrossRef](#)]
48. Denecke, M.A.; Dardenne, K.; Marquardt, C.M. Np(IV)/Np(V) valence determinations from Np L3 edge XANES/EXAFS. *Talanta* **2005**, *65*, 1008–1014. [[CrossRef](#)] [[PubMed](#)]
49. Den Auwer, C.; Simoni, E.; Conradson, S.; Madic, C. Investigating Actinyl Oxo Cations by X-ray Absorption Spectroscopy. *Eur. J. Inorg. Chem.* **2003**, 3843–3859. [[CrossRef](#)]



© 2019 by the authors. Licensee MDPI, Basel, Switzerland. This article is an open access article distributed under the terms and conditions of the Creative Commons Attribution (CC BY) license (<http://creativecommons.org/licenses/by/4.0/>).